Modeling Wind Tunnel Effects on the Radiation Characteristics of Acoustic Sources

W. Eversman*
University of Missouri—Rolla, Rolla, Missouri
and
K.J. Baumeister†
NASA Lewis Research Center, Cleveland, Ohio

The important features of the acoustic field of a propeller operating within a wind tunnel are modeled. The wind tunnel is taken to be of circular cross section, with the flowfield assumed to be uniform. A finite element formulation based on a Gutin type of propeller theory is used to represent the acoustic source both in the wind tunnel and in a free field for comparison purposes. The information sought is the accuracy with which propeller acoustic directivity on the wind tunnel wall matches directivity measured on a reflecting plane placed near the propeller in the free field. An important analytical result shows that it is not possible to obtain an accurate directivity in the tunnel environment unless the modal cutoff ratio for the source exceeds unity for at least the lowest-order mode generated. This result is verified numerically. Acoustic fields and their corresponding directivities in the wind tunnel and free field are compared for situations in which the cutoff condition is satisfied. Several propeller operating conditions and tunnel Mach numbers of $M=0.0$ and $M=-0.5$ are investigated to determine if the number of cut-on modes or the mean flow convective effects significantly influence the matching of the tunnel and free field directivities. It is generally found that there is little resemblance between the radiated acoustic field in the interior of the wind tunnel and in a comparable region in the free field. However, there is a strong similarity between the acoustic field directivity measured on the wind tunnel wall and that on a sideline in the free field. The tunnel Mach number does not appear to be a decisive consideration in the accuracy of the comparisons over the range considered.

Introduction

THE relatively high fuel economy available from propeller-driven aircraft has renewed interest in high-speed, highly loaded, multiple-blade, turboprop propulsion systems. The undesirable features of community noise and, more important, the high-intensity cabin noise associated with the propeller's supersonic helical tip speeds have stimulated new theoretical and experimental research on the acoustic characteristics of turboprops.

The acoustic testing of propellers at realistic in-flow Mach numbers can be carried out in flight, using a suitably scaled model, or performed in wind tunnels capable of producing high subsonic flow velocities, again using a scale model. Acoustic testing with supersonic helical tip speed propellers has initially been carried out in the 8×6 ft transonic wind tunnel at the Lewis Research Center.[1-6] In testing of this type, a model propeller is driven by an air motor to achieve the appropriate rotational speed. Noise measurements are made through bleed holes with pressure transducers installed flush with the tunnel walls. The test site is essentially a duct containing a noise source represented by the propeller. It is not clear that this test environment will generally produce results for directivity or amplitude that have any relationship to flight test results, although some initial flight to wind tunnel comparisons with the NASA Dryden Jetstar aircraft[7,8] have indicated reasonable agreement.

Dittmar[9] has argued that flow convection and the highly directional nature of a typical propeller noise source will minimize reverberation effects when the tunnel Mach number is greater than 0.6. In general, tunnel measurements of sound amplitude and directionality of a propeller depend on such parameters as tunnel flow speed and size, as well as sound frequency and source directivity.

It is the purpose of the present investigation to model mathematically the essential features of the acoustic radiation from propellers in a duct and in free space in order to quantify the success with which duct testing can be expected to approximate freefield conditions.

Because of the importance of source directionality, a detailed model is considered that consists of a finite element representation of the Gutin propeller theory[10] valid in both the near and far field. This model has been implemented in the free field and in the duct environment. The finite element model has been used because it is intended to extend the solution to include the effects of tunnel wall boundary layers, eliminating the possibility of using analytical approaches. In the process of the development of the numerical scheme, advances in the application of the finite element scheme have been made in connection with the modeling of the Gutin acoustic dipole distributions and in the representation of reflection-free duct terminations.

Mathematical Model

The propeller in the wind tunnel test environment is modeled using a Gutin propeller representation[10] in a circular duct of uniform cross section. It is recognized that because propeller testing is done in facilities previously used for other types of testing, the ideal situation presented by a circular geometry is often replaced by a square, a rectangular, or even an octagonal cross section. The three-dimensional character of the acoustic field of a propeller in the circular geometry is much more economically modeled than in other cross sections.

Presented as Paper 84-2364 at AIAA/NASA 9th Aeroacoustics Conference, Williamsburg, VA, Oct. 15-17, 1984; received Jan. 29, 1985; revision received Jan. 8, 1986.

*Curators' Professor. Associate Fellow AIAA.

†Aerospace Engineer.

It is not believed that general conclusions drawn by using this simpler geometry will be fundamentally altered in the other geometries.

In the Gutin representation the propeller is replaced by rotating dipoles in the propeller disk. In this section the governing acoustic equations are presented for an acoustic analogy based on a dipole distribution in cylindrical coordinates. The circular wind tunnel geometry is shown in Fig. 1, as is the cylindrical coordinate system appropriate for this analysis.

The mathematical model has been given in detail in another paper,[11] and the results are repeated here. In terms of nondimensional quantities the propagation of harmonic acoustic disturbances in a circular duct with hard walls is governed by the convected wave equation

$$\nabla^2 p - \left(i\eta_r + M\frac{\partial}{\partial x}\right)^2 p = \nabla \cdot f \tag{1}$$

or

$$\nabla^2 p - 2i\eta_r M\frac{\partial p}{\partial x} - M^2 \nabla \cdot \frac{\partial p}{\partial x} i + \eta_r^2 p = \nabla \cdot f \tag{2}$$

where, consistent with a Gutin-type propeller theory, the acoustic analogy representing the propeller requires a distribution of body forces with no volume sources (these would be required if blade thickness were to be modeled). The nondimensionalization begins with the dimensional pressure p^*, density ρ^*, and velocity V^* and introduces their nondimensional equivalents, where pressure is scaled by $\rho_0 c^2$, density by ρ_0, and velocity by c. ρ_0 and c_0 are reference values of the fluid density and speed of sound. In addition, lengths are scaled by the duct radius R_d, time is scaled by R_d/c, and the body force is scaled by c^2/R_d. The mean flow Mach number is M and the nondimensional frequency is $\eta_r = \omega R_d/c$, where ω is the driving frequency.

Equation (1) or (2), with a suitable body force distribution, is consistent with the Gutin theory, as modified for uniform flow effects by Garrick and Watkins[12]. In the case of radiation of propeller noise to a free field, solutions are obtained in a cylindrical coordinate system with a far-field radiation boundary condition. When the propeller is inside a circular duct with hard walls, a boundary condition of zero normal acoustic velocity (or, equivalently, zero normal pressure derivative) must be enforced at the duct wall. Equations (1) or (2) are thus supplemented by the condition

$$\frac{\partial p}{\partial r} = 0, \qquad r = 1$$

The duct is modeled as infinite in length, requiring that the "terminations" at $x=0$ and $x=L$ be reflection-free. This is most easily enforced by requiring that at the duct terminations the acoustic propagation is given in terms of outgoing acoustic modes. At $x=0$,

$$p(0,r,\theta,t) = \sum_\nu a_\nu^- J_\mu(\kappa_{\mu\nu} r) e^{i\eta_r t} e^{-i\mu\theta}$$

$$\frac{\partial p}{\partial x}(0,r,\theta,t) = \sum_\nu (-ik_{x_{\mu\nu}}^-) a_\nu^- J_\mu(\kappa_{\mu\nu} r) e^{i\eta_r t} e^{-i\mu\theta}$$

and at $x=L$,

$$p(L,r,\theta,t) = \sum_\nu b_\nu^+ J_\mu(\kappa_{\mu\nu} r) e^{i\eta_r t} e^{-i\mu\theta}$$

$$\frac{\partial p}{\partial x}(L,r,\theta,t) = \sum_\nu (-ik_{x_{\mu\nu}}^+) b_\nu^+ J_\mu(\kappa_{\mu\nu} r) e^{i\eta_r t} e^{-i\mu\theta}$$

$J_\mu(\kappa_{\mu\nu} r)$ is the Bessel function of the first kind of order μ with argument $\kappa_{\mu\nu} r$. $\kappa_{\mu\nu}$ are solutions of

$$J'_\mu(\kappa_{\mu\nu}) = 0$$

The axial wave number $k_{x_{\mu\nu}}$ is given by

$$\frac{k_{x_{\mu\nu}}}{\eta_r} = \frac{1}{1-M^2}\left[-M \pm \sqrt{1-(1-M^2)\left(\frac{\kappa_{\mu\nu}}{\eta_r}\right)^2}\right] \tag{3}$$

and the distinction between $k_{x_{\mu\nu}}^+$ and $k_{x_{\mu\nu}}^-$ (corresponding to propagation in the positive or negative x direction) is determined by the sign choice. The positive sign corresponds to propagation in the positive x direction and for cut-on modes $[(1-M^2)(\kappa_{\mu\nu}/\eta_r)^2 < 1]$. The opposite is true for cutoff modes.

The body forces appearing in Eq. (1) or (2) appropriate to the Gutin theory have also been discussed in another paper.[11] For a propeller rotating in the positive sense with respect to the x axis in Fig. 1, the x and θ components of the nondimensional body force applied by the propeller to the fluid are

$$f_x = -\frac{N\Omega}{2\pi}\frac{1}{\rho_0 c^2}\left(\frac{\ell_p(r)}{a}\right)\delta(x)\sum_{m=-\infty}^{m=\infty} \times \sin(mN\Omega\tau)\tau \exp\left[imN\left(\frac{\Omega R_d}{c}t-\theta\right)\right]\Big/ mN\Omega \tag{4}$$

$$f_\theta = \frac{N\Omega}{2\pi}\frac{1}{\rho_0 c^2}\left(\frac{\ell_T(r)}{a}\right)\delta(x)\sum_{m=-\infty}^{m=\infty} \times \sin(mN\Omega\tau)\tau \exp\left[imN\left(\frac{\Omega R_d}{c}t-\theta\right)\right]\Big/ mN\Omega \tag{5}$$

where N is the number of blades, Ω the angular velocity of the propeller (rad/s), $\ell_p(r)$ and $\ell_T(r)$ the propulsive and torque components of the blade lift per unit span, a the projection of the blade chord on the propeller disk, and τ the acoustic pulse duration as the propeller passes a fixed point ($\tau = a/\Omega r^*$, r^* = dimensional radius). The body force is seen to consist of the fundamental tone at nondimensional frequency

$$\eta = \frac{N\Omega R_d}{c}$$

and angular mode $\mu = \pm N$ and harmonics with frequency

$$\eta_m = \eta_r = m_\eta$$

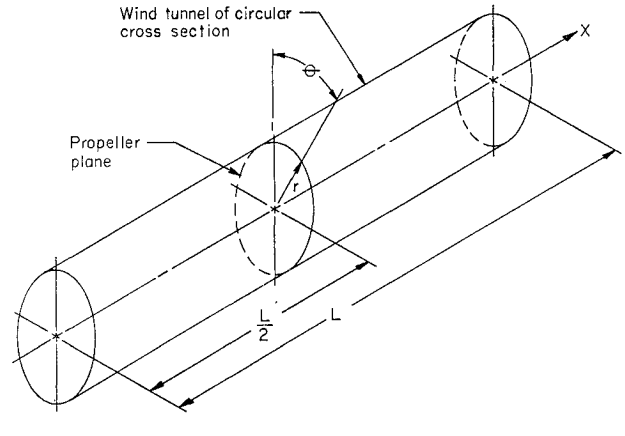

Fig. 1 Geometry of the propeller in a circular wind tunnel.

and angular mode $\mu = \pm mN$. Specific angular harmonics of the body forces are written as

$$f_{x_m}(x,r,\theta,t) = F_{x_m}(r)\exp[i(\eta_m t - \mu\theta)]$$

and

$$f_{\theta_m}(x,r,\theta,t) = F_{\theta_m}(r)\exp[i(\eta_m t - \mu\theta)]$$

where

$$F_{x_m} = -\frac{N\Omega}{2\pi}\frac{1}{\rho_0 c^2}\left(\frac{\ell_p(r)}{a}\right)\frac{\sin(mn\Omega\tau)}{mN\Omega}\delta(x) \qquad (6)$$

and

$$F_{\theta_m} = \frac{N\Omega}{2\pi}\frac{1}{\rho_0 c^2}\left(\frac{\ell_T(r)}{a}\right)\frac{\sin(mn\Omega\tau)}{mN\Omega}\delta(x) \qquad (7)$$

The right-hand side in Eq. (1) is constructed by use of the divergence operation in cylindrical coordinates

$$\nabla\cdot f = \frac{\partial f_x}{\partial x} + \frac{1}{r}\frac{\partial}{\partial r}(rf_r) + \frac{1}{r}\frac{\partial f_\theta}{\partial\theta}$$

For the mth Fourier angular component for the harmonic forcing function at $\eta_r = mN\Omega R_d/c$

$$\nabla\cdot f = \frac{\partial F_x}{\partial x} - i\frac{\mu}{r}F_\theta$$

At a given radius r, the right-hand side of Eq. (1) has the form

$$\nabla\cdot f = A_p\frac{\partial}{\partial x}[\delta(x)] + iA_T\delta(x) \qquad (8)$$

This represents the combination of a dipole and a simple source.

An Exact Solution

The Green's function for Eq. (1) is the solution of

$$(1-M^2)\frac{\partial^2 p}{\partial x^2} + \frac{\partial^2 p}{\partial r^2} + \frac{1}{r}\frac{\partial p}{\partial r} + \frac{1}{r^2}\frac{\partial^2 p}{\partial\theta^2}$$

$$-2i\eta_r M\frac{\partial p}{\partial x} + \eta_r^2 p = \delta(x)\delta(r-r_0)e^{-i\mu\theta}$$

An eigenfunction expansion can be used to generate the solutions

$$P(x,r) = \frac{i}{1-M^2}\sum_n \frac{J_\mu(\kappa_{\mu n})}{N_{\mu nn}}$$

$$\times\frac{1}{k_{x_n}^+ - k_{x_n}^-}J_\mu(\kappa_{\mu n}r)\exp(-ik_{x_n}^+ x), \qquad x>0$$

$$P(x,r) = \frac{i}{1-M^2}\sum_n \frac{J_\mu(\kappa_{\mu n})}{N_{\mu nn}}$$

$$\times\frac{1}{k_{x_n}^+ - k_{x_n}^-}J_\mu(\kappa_{\mu n}r)\exp(-ik_{x_n}^- x), \qquad x<0 \qquad (9)$$

where, simplifying previous notation,

$$k_{x_n}^\pm = k_{x\mu n}^\pm$$

and

$$N_{\mu nn} = \int_0^1 rJ_\mu^2(\kappa_{\mu n}r)\,dr$$

The solution for a right-hand side that contains $\delta'(x-x_0)$ is easily determined by differentiation to be

$$P(x,r) = \frac{1}{1-M^2}\sum_n \frac{J_\mu(\kappa_{\mu n})}{N_{\mu nn}}$$

$$\times\frac{k_{x_n}^+}{k_{x_n}^+ - k_{x_n}^-}J_\mu(\kappa_{\mu n}r)\exp(-ik_{x_n}^+ x), \qquad x>0$$

$$P(x,r) = \frac{1}{1-M^2}\sum_n \frac{J_\mu(\kappa_{\mu n})}{N_{\mu nn}}$$

$$\times\frac{k_{x_n}^-}{k_{x_n}^+ - k_{x_n}^-}J_\mu(\kappa_{\mu n}r)\exp(-ik_{x_n}^- x), \qquad x<0 \qquad (10)$$

For a forcing function of the form of Eq. (8), Eqs. (9) and (10) show that solutions will be

$$P(x,r) = \frac{1}{1-M^2}\sum_n \frac{J_\mu(\kappa_{\mu n})}{N_{\mu nn}}$$

$$\times\left[\frac{A_p k_{x_n}^+ - A_T}{k_{x_n}^+ - k_{x_n}^-}\right]J_\mu(\kappa_{\mu n}r)\exp(-ik_{x_n}^+ x), \qquad x>0$$

$$P(x,r) = \frac{1}{1-M^2}\sum_n \frac{J_\mu(\kappa_{\mu n})}{N_{\mu nn}}$$

$$\times\left[\frac{A_p k_{x_n}^- - A_T}{k_{x_n}^+ - k_{x_n}^-}\right]J_\mu(\kappa_{\mu n}r)\exp(-ik_{x_n}^- x), \qquad x<0 \qquad (11)$$

Directivity When All Modes are Cut Off

From Eqs. (11) an important conclusion can be drawn about source directivity when the propeller noise source is

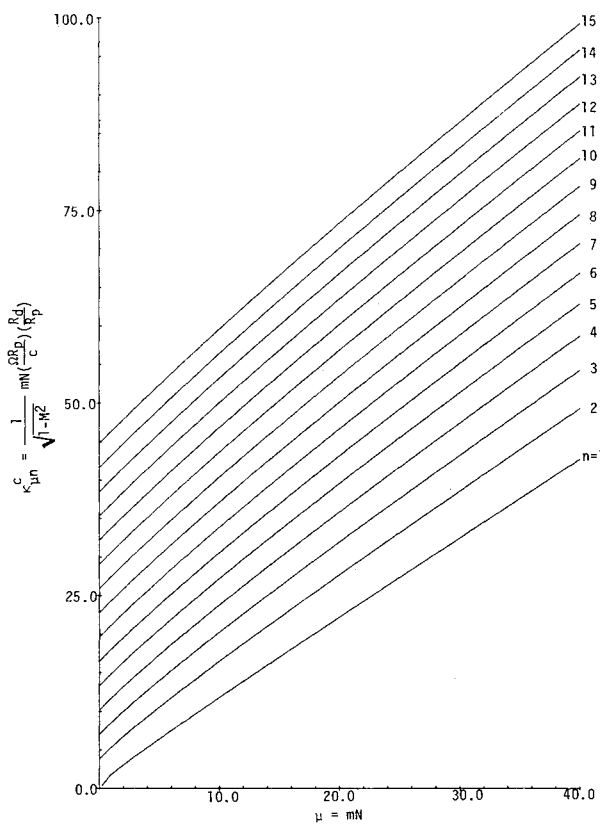

Fig. 2 Modal propagation map for a propeller in a circular wind tunnel. The nth radial mode propagates for the μth angular mode if $\kappa_{\mu n}^c$ lies above the n curve.

operating so that no cut-on modes are present. Equation (3) defining the wave numbers shows that in general $k_{x_n}^{\pm}$ can be written

$$k_{x_n}^{\pm} = -\gamma + \delta_{\mu n}^{\pm}$$

where γ is real and independent of the particular mode and

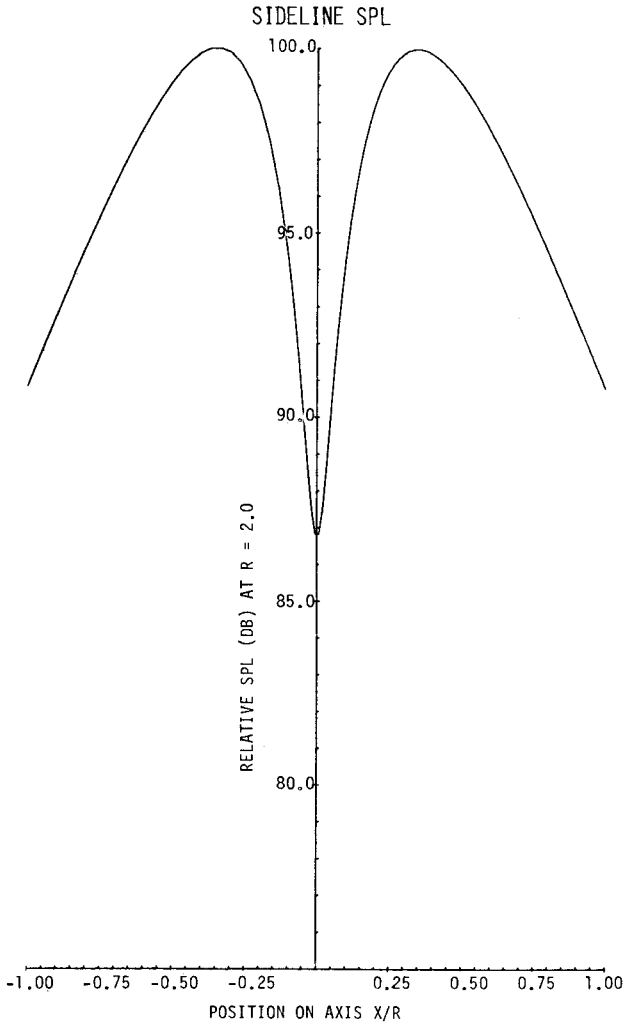

Fig. 3 Contours of constant acoustic pressure amplitude in an x-r plane for the fundamental tone of a two-blade propeller in a circular wind tunnel with $M=-0.5$ and below the first radial mode cut-on $\mu=2$, $\eta_r=2.0$ (duct), $R=$ duct radius.

$\delta_{\mu n}^{\pm}$ can be real or imaginary. $\delta_{\mu n}^{\pm}$ is real if

$$(1-M^2)(\kappa_{\mu n}/\eta_r)^2 < 1$$

and the mode is cut on. Otherwise the mode is cut off and $\delta_{\eta n}$ is imaginary. For cut-on modes

$$\delta_{\mu n}^{\pm} = \pm\eta_r\sqrt{1-(1-M^2)(\kappa_{\mu n}/\eta_r)^2} = \pm\alpha_{\mu n}$$

and for cut-off modes

$$\delta_{\mu n}^{\pm} = \pm i\eta_r\sqrt{(1-M^2)(\kappa_{\mu n}/\eta_r)^2 - 1} = \pm i\beta_{\mu n}$$

Equations (11) are now written

$$P(x,r) = \frac{ie^{-i\gamma x}}{1-M^2}\sum_n \frac{J_\mu(\kappa_{\mu n})}{N_{\mu nn}} \times \left[\frac{A_p(-\gamma+\delta_{\mu n}^{+})-A_T}{\delta_{\mu n}^{+}-\delta_{\mu n}^{-}}\right] J_\mu(\kappa_{\mu n}r)\exp(-i\delta_{\mu n}^{+}x), \qquad x>0$$

$$P(x,r) = \frac{ie^{-i\gamma x}}{1-M^2}\sum_n \frac{J_\mu(\kappa_{\mu n})}{N_{\mu nn}} \times \left[\frac{A_p(-\gamma+\delta_{\mu n}^{-})-A_T}{\delta_{\mu n}^{+}-\delta_{\mu n}^{-}}\right] J_\mu(\kappa_{\mu n}r)\exp(-i\delta_{\mu n}^{-}x), \quad x<0 \qquad (12)$$

It is noted that if some modes are cut on, $P(x,r)$ has no symmetry properties, that is $P(x,r)$ bears no special relation to $P(-x,r)$. However, if all modes are cut off, then

$$P(x,r) = \frac{e^{-i\gamma x}}{1-M^2}\sum_n \frac{J_\mu(\kappa_\mu n)}{N_{\mu nn}} \times \left[\frac{A_p(\gamma+i\beta_{\mu n})+A_T}{2\beta_{\mu n}}\right] J_\mu(\kappa_{\mu n}r)\exp(-\beta_{\mu n}x), \qquad x>0$$

$$P(x,r) = \frac{e^{-i\gamma x}}{1-M^2}\sum_n \frac{J_\mu(\kappa_{\mu n})}{N_{\mu nn}} \times \left[\frac{A_p(\gamma-i\beta_{\mu n})+A_T}{2\beta_{\mu n}}\right] J_\mu(\kappa_{\mu n}r)\exp(+\beta_{\mu n}x), \quad x<0 \qquad (13)$$

In this case it is seen that $P(-x,r)=P^*(x,r)$, where the superscript (*) represents the complex conjugate. The significance is that the pressure magnitude becomes an even or symmetric function in x. This makes it impossible to

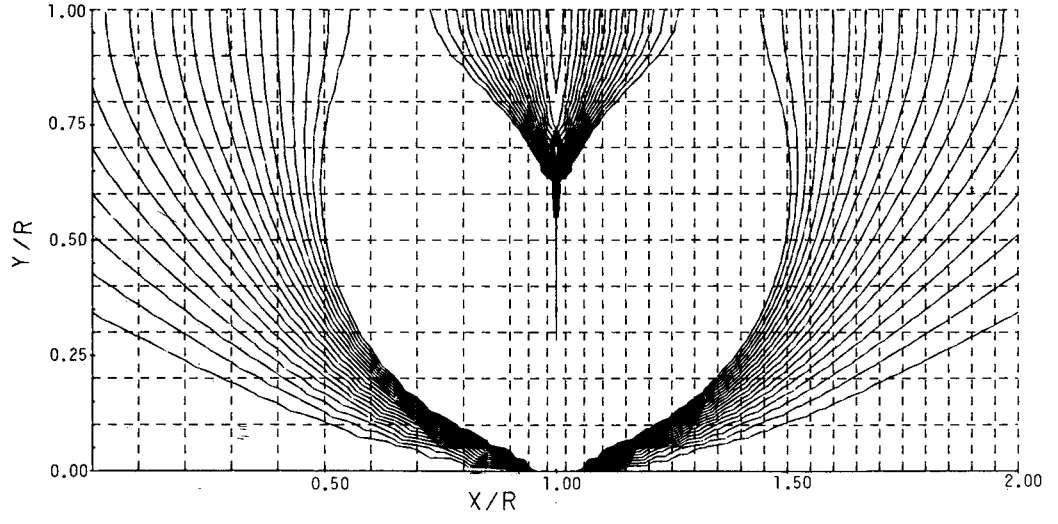

Fig. 4 Fundamental tone acoustic directivity on the duct wall near the two-blade propeller below first radial mode cut-on with $M=-0.5$. $\mu=2$, $\eta_r=2.0$ (duct).

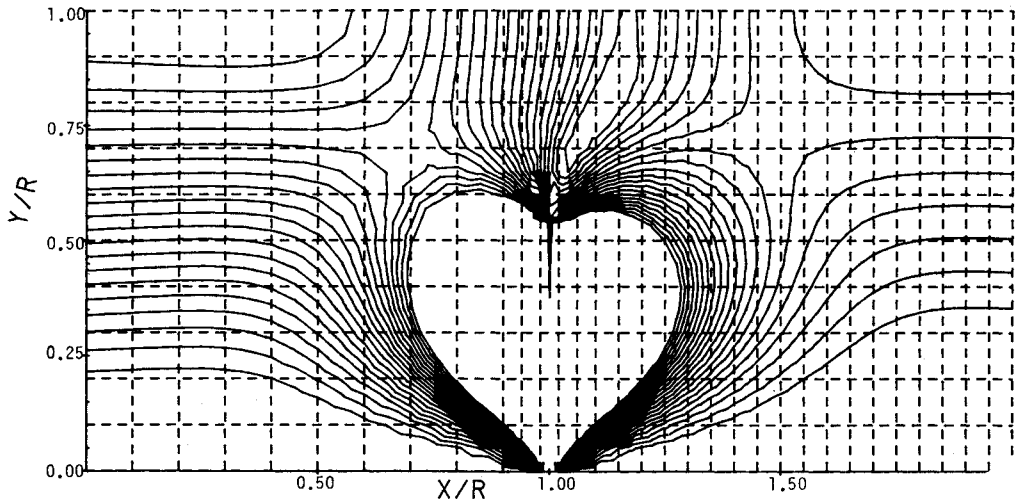

Fig. 5 Contours of constant acoustic pressure amplitude in an x-r plane for the fundamental tone of a two-blade propeller in a circular wind tunnel with $M=0.0$ and with the first radial mode cut on. $\mu=2$, $\eta_r=4.0$ (duct), $R=$ duct radius.

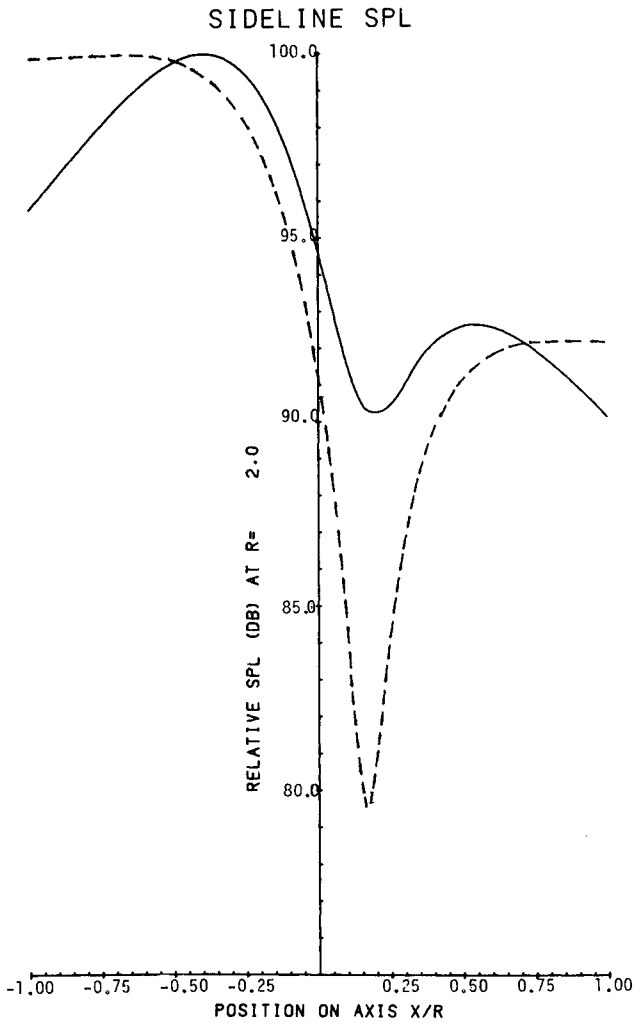

Fig. 6 Fundamental tone acoustic directivity at the location of the duct wall near the two-blade propeller with one radial mode propagating and with $M=0.0$. $\mu=2$, $\eta_r=4.0$ (duct). The dashed line is the in-duct calculation and the solid line is the free-field calculation; $R=$ duct radius.

duplicate the directivity of the propeller source in the duct if the propeller geometry and operational parameters excite only cut-off modes, for when only cut-off modes are present, the duct pressure amplitude field is symmetric.

The key consideration is the mode cutoff ratio[13]

$$\xi=\kappa^c_{\mu n}/\kappa_{\mu n}$$

where

$$\kappa^c_{\mu n}=\eta_r/[(1-M^2)^{1/2}]$$

The frequency of excitation η_r depends on the rotational frequency, the number of blades, and the harmonic in question

$$\eta_r=mN\Omega R_d/c$$

The value of $\kappa^c_{\mu n}$ depends on the number of blades and the harmonic through the eigenvalue equation.

$$J'_\mu(\kappa_{\mu n})=0, \qquad \mu=mN$$

Figure 2 is a plot $\kappa^c_{\mu n}$ as a function of the angular mode number for several radial mode numbers. The ordinate is given as $\kappa^c_{\mu n}$ so that the curves become contours of unity cutoff ratio. This can be used to determine what modes are cut on for a given propeller test condition. For example, it can be determined that for a two-bladed propeller the first angular harmonic produces the second angular mode ($m=1$, $mN=2$). This angular mode has no cut-on radial modes unless $\kappa^c_{\mu n}$ exceeds approximately 3.05, as determined from Fig. 2.

The results obtained in this section and summarized in Eqs. (12) and (13) are for a single-ring doublet. The conclusions drawn are valid for the dipole noise of any Gutin propeller since this can be represented by a suitable superposition of ring doublets. Computational evidence of this is given in Figs. 3 and 4, which show results of a finite element model of the propeller in the duct in the presence of mean flow. The test condition modeled is that of a two-bladed propeller in a duct with radius twice that of the propeller. The nondimensional propeller rotational frequency based on propeller radius is $\Omega R_p/c=0.5$. The first harmonic thus produces $mN\Omega R_p/c=1.0$. Based on duct radius, this produces

$$\eta_r=(mN\Omega R_p/c)(R_d/R_p)=2.0$$

From Fig. 2, it is seen that at $mN=2$ with $M=-0.5$ the test condition is below the $n=1$ unity cut-off ratio curve and, therefore, there are no cut-on modes present. Figure 3 shows contours of constant pressure magnitude for the case of flow at $M=-0.5$. The radiation pattern is symmetric as verified by Fig. 4, which is the plot of directivity along the duct outer wall.

It is clear that the relationship of the propeller test conditions to the cut-off/cut-on frequencies for the wind tunnel is of crucial importance if there is to be any hope of approximating a freefield radiation pattern. It is also clear that the

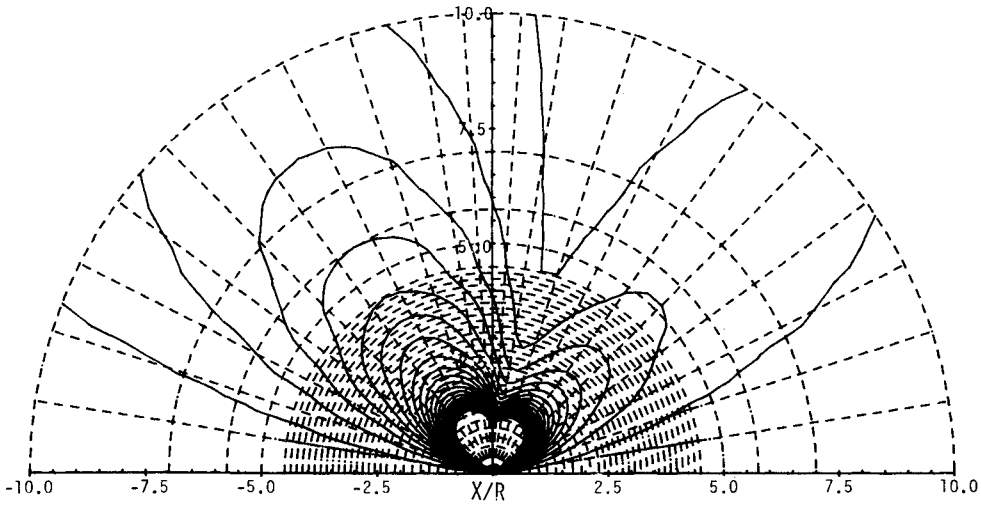

Fig. 7 Contours of constant acoustic pressure amplitude in an x-r plane for the fundamental tone of a two-blade propeller in the free field with $M=0.0$. $\mu=2$, $\eta_r=4.0$ (based on duct radius); $R=$ propeller radius.

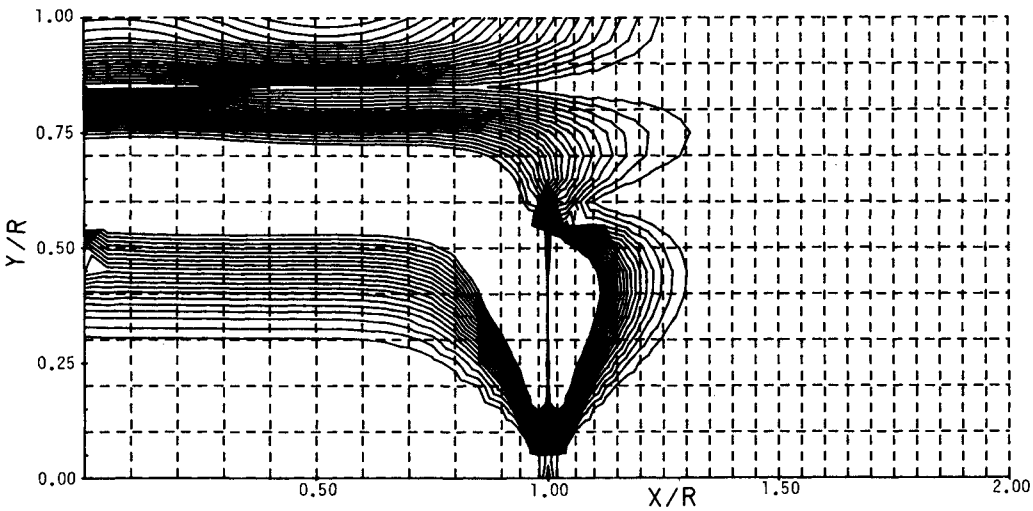

Fig. 8 Contours of constant acoustic pressure amplitude in an x-r plane for the fundamental tone of a six-blade propeller in a circular wind tunnel with $M=0.0$ and with the first two radial modes cut on. $\mu=6$, $\eta_r=12.0$ (duct); $R=$ duct radius.

presence of a mean flow does not alter this conclusion unless the mean flow is of magnitude sufficient to move the test conditions on Fig. 2 above the $n=1$ unity cut-off ratio curve. In the case discussed in the examples of Figs. 3 and 4, the Mach number would have to exced $M=-0.76$ for this to occur.

Directivity Above Cut-off

It has been shown that propeller testing in a duct environment must be carried out so that the harmonic frequency $mn\Omega R_d/c$ exceeds the cut-on frequency for the lowest-order radial mode corresponding to the angular mode $\mu=mN$. Since wind tunnel testing would normally be done to simulate the free field of either a full-scale or model-scale propeller, the frequency parameter to be duplicated would be $mN\Omega R_p/c$. To insure that testing is done with at least one mode cut-on, it is seen that for a given propeller model the ratio R_d/R_p may be of critical importance in the establishment of a satisfactory test condition.

Under the assumption that it is possible to achieve test conditions such that propagating duct modes are cut on, it is now appropriate to determine if directivity measured on the duct wall has any relationship to free-field directivity.

The first calculation to be considered is with no mean flow in the duct. Two propeller configurations are investigated with $R_d/R_p=2.0$. No effort is made to adjust the propeller loading since only the frequency and duct mode effects are sought.

In the first case the propeller of the previous example is considered with $\Omega R_p/c=1.0$. For this two-bladed propeller, the duct nondimensional frequency (based on duct radius) is $\eta_r=4.0$ and only one mode is propagating. Only the first harmonic is calculated. Figure 5 shows contours of constant acoustic pressure amplitude, and a distinct asymmetry is noted. Figure 6 gives the directivity on the duct wall, and this displays a radiation pattern with maximum levels behind the propeller. Also shown on Fig. 6 is the directivity in the free field for the same propeller taken on a line two propeller radii from the axis. Figure 7 shows the contours of constant acoustic pressure amplitude in the free field. The free field calculations were made using the finite element method of Ref. 11, and the in-duct calculations were made using the propeller representation of Ref. 11 but confining it in a circular duct with reflection-free ends, as previously described.

Figures 5 and 7 leave little doubt that the acoustic radiation field is substantially altered by the presence of the duct except perhaps very near the propeller. Figure 6 shows that both the free-field directivity and the in-duct directivity are decidedly asymmetric, with the maximum sound pressure level (SPL) occurring behind the propeller. Both the in-duct and free-field directivity have two distinct lobes and an SPL minimum just ahead of the propeller. The directivities are similar in a region directly over the propeller. On this plot both curves are normalized to 100 dB to enhance the comparison of directivity. As one would expect, the absolute level of the in-duct acoustic environment is higher than the freefield by 9.0 dB. It is important to note that the axial

distance scale is in duct radii so that $x/R_d = \pm 1.0$ covers a 90 deg angle, ± 45 deg on either side of the propeller. This would probably exceed the range over which any similarity between duct directivity and freefield directivity could be expected.

A second example considers a propeller with six blades, $\Omega R_p/c = 1.0$, and no mean flow. For the first harmonic this produces a duct nondimensional frequency $\eta_r = 12.0$, which exceeds the second-mode cut-on value of 11.73. There are thus two radial modes propagating in the sixth angular mode. Figures 8-10 show the in-duct and free-field radiation patterns and directivities. The in-duct and free-field radiation patterns of Figs. 8 and 10 show almost no similarity. However, a comparison of the acoustic field directivity on the duct wall, Fig. 9, reveals a distinct similarity in a narrow region over the propeller. The aft lobe is better represented in the duct than is the forward lobe. The overall comparison is not as favorable as in the two-bladed propeller case. Again, the directivities shown on Fig. 10 are normalized to 100 dB. In this case, the in-duct level is 13.0 dB higher than in the freefield.

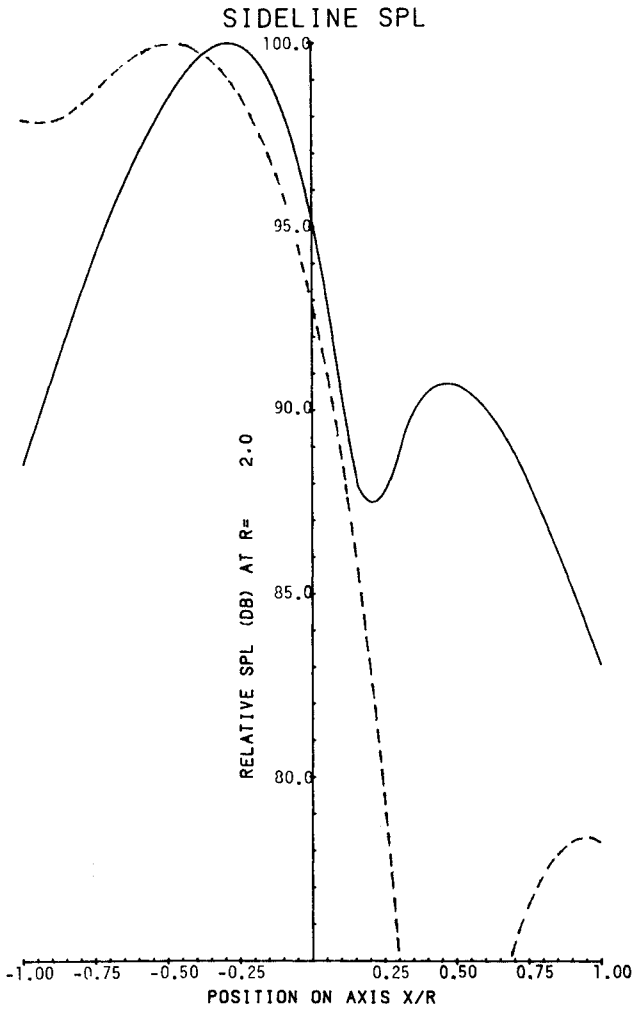

Fig. 9 Fundamental tone acoustic directivity at the location of the duct wall near the six-blade propeller with two radial modes propagating and with $M = 0.0$. $\mu = 6$, $\eta_r = 12.0$ (duct). The dashed line is the in-duct calculation and the solid line is the free-field calculation; $R =$ duct radius.

From the results with no mean flow, it can be said that in-duct and free-field directivities measured in a region on the wall directly over the propeller show qualitatively similar trends and that the major characteristics are well represented. A strong influence of the number of propagating modes is not observed, although the radiation pattern in the duct interior and the directivity on the wall is less representative of the free field when a second duct mode is cut on.

The presence of flow in the duct is investigated by consideration of the two-bladed propeller at $\Omega R_p/c = 1.0$, which produces $\eta_r = 4.0$ in the duct. A Mach number of $M = -0.5$ (directed toward the propeller) has been assumed. Figures 11-13 show the results of these calculations. The radiation pattern near the propeller in Fig. 11 is representative of typical free-field patterns, but nearer the wall the pattern shows substantial effects of the presence of the wall. Figure 12 shows the comparison of free-field and in-duct directivity on the duct wall. As in previous cases, both curves are normalized to 100 dB. The important effects are again certainly reproduced, with the quality of the comparison depending on the choice of base levels for the curves. The quality of the comparison is not significantly different than when flow is absent in the two-bladed case. The in-duct levels are 6.5 dB above the free field. Calculations in the free field, Fig. 12, were carried out on a skewed mesh, which in the far field allows the convenient implementation of the radiation condition in the presence of uniform mean flow.

In this case no influence of Mach number on the comparison between the in-duct and freefield calculations is observed. The Mach number in this case does not introduce a second propagating duct mode. Based on the calculations discussed here, it is concluded that in order to have any similarity between the wind tunnel acoustic field and the acoustic field in free-field testing, it is necessary that at least one duct mode be cut on. The presence of more than one duct mode appears to confuse the comparison in the duct in-

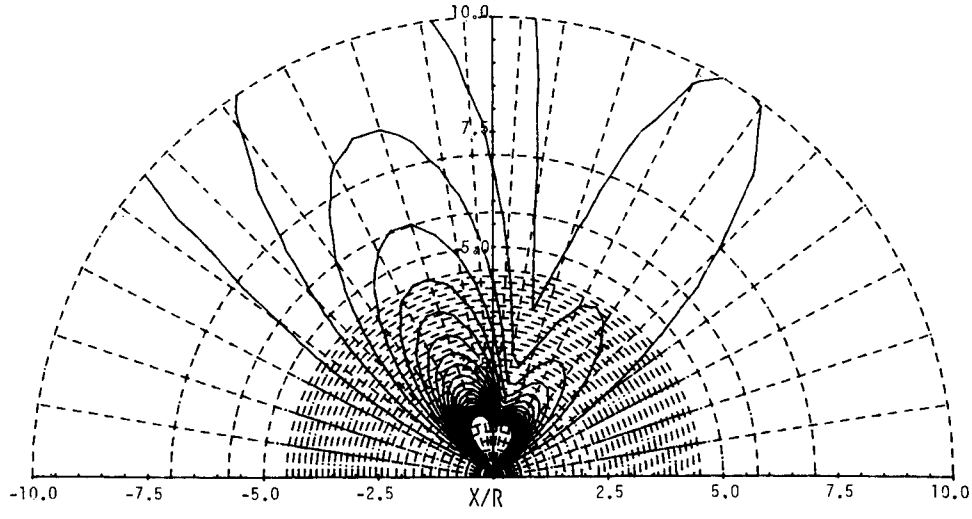

Fig. 10 Contours of constant acoustic pressure amplitude in an x-r plane for the fundamental tone of a six-blade propeller in the free field with $M = 0.0$. $\mu = 6$, $\eta_r = 12.0$ (based on duct radius); $R =$ propeller radius.

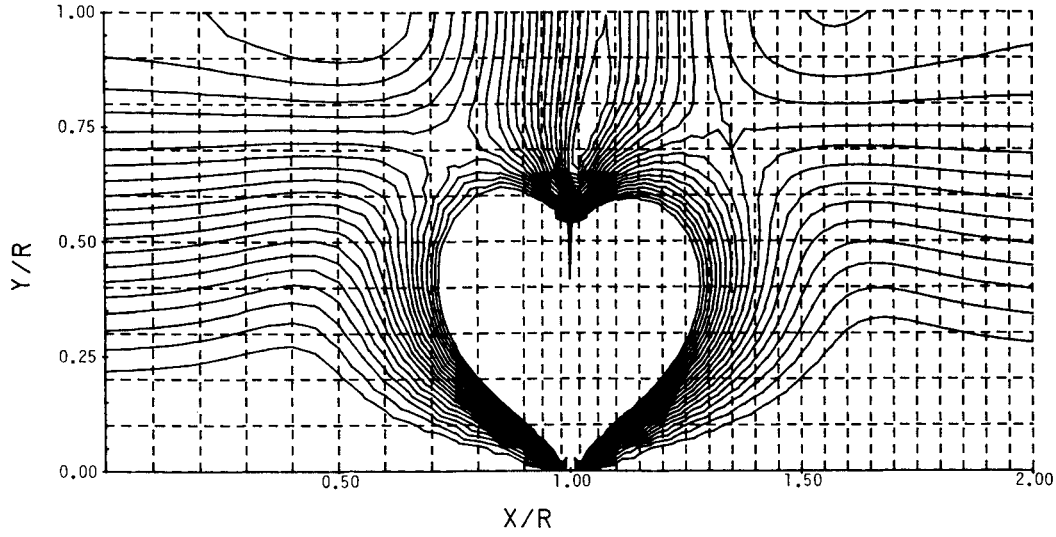

Fig. 11 Contours of constant acoustic pressure amplitude in an x-r plane for the fundamental tone of a two-blade propeller in a circular wind tunnel with $M=-0.5$ and with the first radial mode cut on. $\mu=2$, $\eta_r=4.0$ (duct); $R=$duct radius.

terior, but a meaningful comparison of directivity on the duct wall near the propeller is still possible. The Mach number in the duct has no apparent effect except as it may alter the number of propagating modes.

Comments on a Real Test Situation—The SR3 Propeller

Dittmar and Lasagna[8] have made comparisons between wind tunnel and in-flight acoustic measurements for a scale-model SR-3 propeller. The in-flight measurements were made using the NASA Dryden Research Center Jetstar aircraft with the propeller mounted on a pylon above the fuselage. The propeller was driven by an air turbine operating on bleed air. Measurements were made on the fuselage on a line directly under the centerline of the propeller.

Wind tunnel tests were made on the same propeller in the NASA Lewis Research Center 8×6 ft transonic wind tunnel. Acoustic measurements were made on the wind tunnel walls. The propeller geometrical and operational data are as follows: rotational speed, $\Omega=783.6$ rad/s; propeller radius, $R_p=1.021$ ft; speed of sound, $c=1125$ ft/s (assumed); number of blades, $N=8$; and tunnel Mach number, $M=0.8$. The wind tunnel cross-sectional area is 48 ft^2, which for the modeling approach used in this investigation is taken as equivalent to a circular tunnel with the same area. The equivalent tunnel radius is then $R_d=3.91$ ft. For the first angular harmonic $\mu=mN=(1)(8)$, the nondimensional frequency for the propeller, based on the propeller radius, is

$$\eta_{rp}=mN(\Omega R_p/c)=5.7$$

Based on the equivalent duct radius

$$\eta_{rd}=mN(\Omega R_p/c)\,(R_d/R_p)=21.8$$

It is also found that

$$\kappa^c_{\mu m}=\frac{mn(\Omega R_p/c)\,(R_d/R_p)}{\sqrt{1-M^2}}=36.3$$

Reference to Fig. 2 reveals that eight radial modes will be cut on and that, based on what we have been able to deduce computationally so far, the test conditions are appropriate for at least a qualitative reproduction of the freefield directivity on the duct wall. It is intended that cases of this complexity be modeled in future investigations.

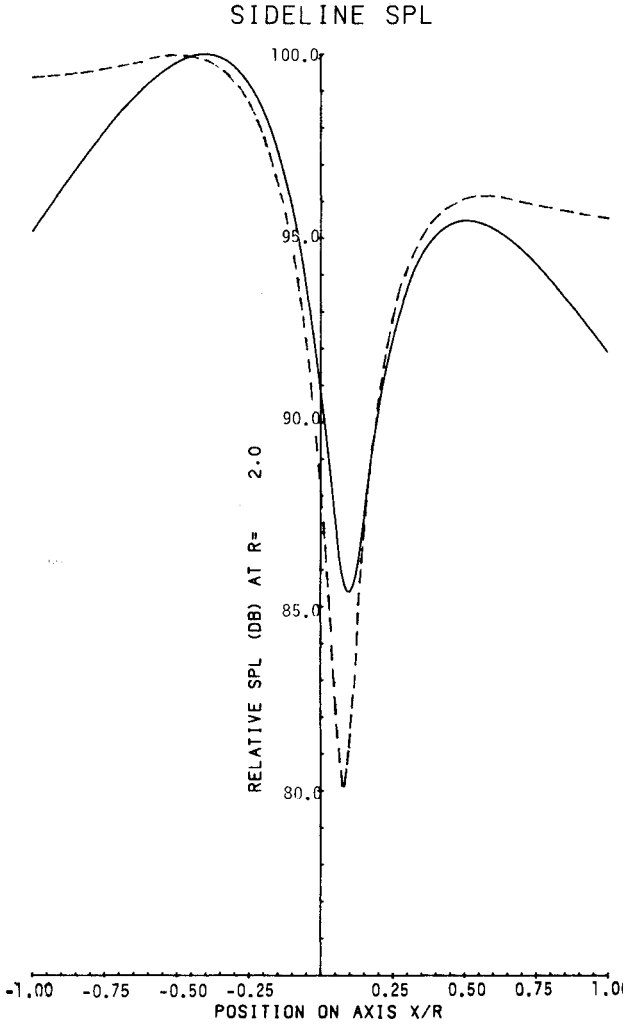

Fig. 12 Fundamental tone acoustic directivity at the location of the duct wall near the two-blade propeller with one radial mode propagating and with $M=-0.5$. $\mu=2$, $\eta_r=4.0$ (duct). The dashed line is the in-duct calculation and the solid line is the free-field calculation; $R=$duct radius.

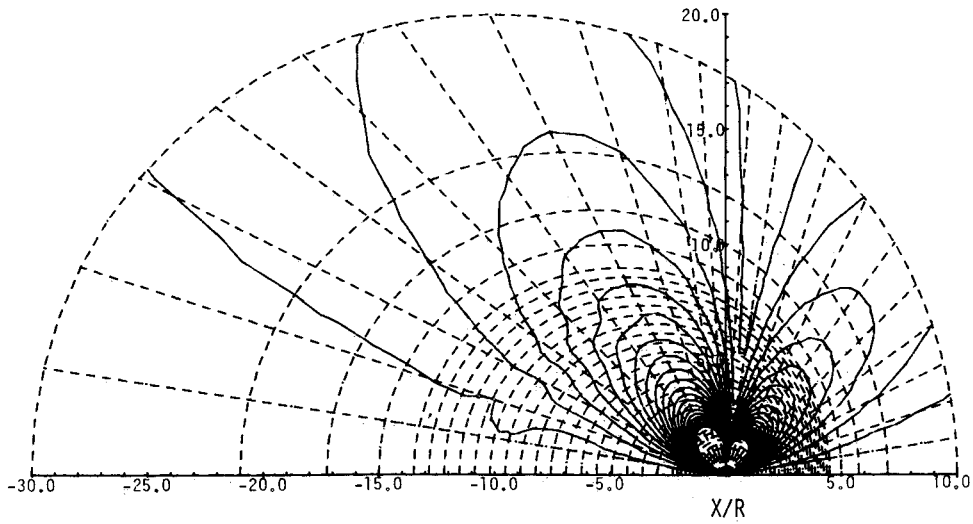

Fig. 13 Contours of constant acoustical pressure amplitude in an x-r plane for the fundamental tone of a two-blade propeller in the free field with $M=-0.5$. $\mu=2$, $\eta_r=4.0$ (based on duct radius); R = propeller radius.

Observations

The finite element modeling method discussed and applied in this investigation has provided very useful insight into the radiation directivity of propellers in the free field and enclosed in ducts. It has been shown that, at least for the situations considered, some important features of the free-field directivity can be approximated in the wind tunnel environment with or without flow. However, we do offer the reservation that the range of parameters considered is extremely limited. In fact, the range of parameters, such as R_d/R_p, $\Omega R_p/c$, m, N, propeller loading, and tunnel Mach number, probably preclude any general quantification beyond our first observation on the importance of the modal cut-off ratio.

The modeling method considered here should be used in advance of a test to determine the extent to which the tunnel environment can be expected to approximate the free-field conditions. It is relatively simple to implement and inexpensive to use and has potential for growth in the sophistication of the propeller and duct modeling.

References

[1]Dittmar, J.H., Blaha, B.J., and Jeracki, R.J., "Tone Noise of Three Supersonic Helical Tip Speed Propellers in a Wind Tunnel at 0.8 Mach Number," NASA TM-79046, 1978.

[2]Dittmar, J.H., Jeracki, R.J., and Blaha, B.J., "Tone Noise of Three Supersonic Helical Tip Speed Propellers in a Wind Tunnel," NASA M-79167, 1979.

[3]Dittmar, J.H. and Jeracki, R.J., "Additional Noise Data on the SR-3 Propeller," NASA TM-81736, 1981.

[4]Dittmar, J.H., Stefko, G.L., and Jeracki, R.J., "Noise of the 10-Bladed, 40° Swept SR-6 Propeller in a Wind Tunnel," NASA TM-82950, 1982.

[5]Dittmar, J.H., Stefko, G.L., and Jeracki, R.J., "Noise of the 10-Bladed, 60° Swept SR-5 Propeller in a Wind Tunnel," NASA TM-83054, 1983.

[6]Dittmar, J.H. and Jeracki, R.J., "Noise of the SR-3 Propeller Model at 2° and 4° Angle of Attack," NASA TM-82738, 1981.

[7]Mackall, K.G., Lasagna, P.L., Walsh, K., and Dittmar, J.H., "In-Flight Acoustic Results from an Advanced-Design Propeller at Mach Numbers to 0.8," AIAA Paper 82-1120, 1982.

[8]Dittmar, J.H. and Lasagna, P.L., "A Preliminary Comparison Between the SR-3 Propeller Noise in Flight and in a Wind Tunnel," NASA TM-82805, 1982.

[9]Dittmar, J.H., "Why Credible Propeller Noise Measurements Are Possible in the Acoustically Untreated NASA Lewis 8 Foot by 6 Foot Wind Tunnel," *Journal of the Acoustical Society of America*. Vol. 75, June 1984, pp. 1913-1914.

[10]Gutin, L., "On the Sound Field of a Rotating Propeller," NACA TM 1195, 1948, (translated from the 1936 Russian version).

[11]Eversman, W. and Steck, J.E., "Finite Element Modelling of Acoustic Singularities with Application to Near and Far Field Propeller Noise," AIAA Paper 84-2286, 1984.

[12]Garrick, I.E. and Watkins, C.E., "A Theoretical Study of the Effect of Forward Speed on the Free Space Sound Pressure Field Around Propellers," NACA TR 1198, 1953.

[13]Rice, E.J. and Heidmann, M.F., "Modal Propagation Angles in a Cylindrical Duct with Flow and Their Relation to Sound Radiation," AIAA Paper 79-0183, 1979.